Experimental and Numerical Study on Liquid Cooling Battery Thermal Management System for Battery Electric Vehicles

- Analysis of electrical and coolant parameters -

Maram Rihawi [1] Kamaleshwar Nandagopal [1] Ratnak Sok [1, *] Jin Kusaka [1]

1) Propulsion and Energy Systems Laboratory, Waseda University, Shinjuku, Tokyo, Japan

*E-mail: * ratnak@ruri.waseda.jp*

ABSTRACT: Thermal management of lithium-ion battery modules is essential to prevent overheating and thermal runaway. This study analyzed the thermal and pressure responses of a liquid-cooled battery pack under varying discharge currents (150 A vs. 50 A) and ambient temperatures (30°C vs. -5°C). Higher currents led to rapid temperature increases, requiring intensified cooling, while lower temperatures reduced pressure stability, emphasizing the need for adaptable thermal management. A numerical model extended the experimental analysis by incorporating a refrigerant and cabin circuit into a validated coolant circuit. Under a constant discharge case at 12°C ambient temperature with 100 A, the numerical results showed that the cabin temperature increased from 12°C to 25°C within 800 seconds. This validated the system's effectiveness in maintaining optimal thermal conditions.

KEY WORDS: Electric vehicle, Thermal management system, Parametric study.

1. INTRODUCTION

The transition to battery electric vehicles (BEVs) is driven by increasingly stringent pollution regulations and the global ambition to achieve carbon neutrality. Lithium-ion batteries (LIBs), with their high energy density and power capability, have become the primary energy storage solution for BEVs. However, maintaining the thermal stability of LIBs under various ambient and climatic conditions remains a challenge, as temperature imbalances within the battery pack can affect performance, safety, and overall driving range [1].

Previous studies have established that non-uniform temperature distribution across battery bricks, modules, and packs can lead to performance degradation and increased thermal stress [2]. Understanding these temperature variations under real-world conditions is essential for developing efficient battery thermal management systems (BTMS) that support the long-term durability of BEVs. [3].
This research investigates the thermal behavior of a mid-size fully battery-electric SUV during chassis dynamometer testing, focusing on both discharge and pressure drop cycles. The experimental setup includes a liquid cooling system and detailed temperature monitoring across different battery components. By evaluating battery voltage, current, temperature distribution, pressure drop, and coolant flow rate, this study seeks to provide insights into how varying initial conditions (ambient temperature, initial cell temperature, and initial state of charge) influence thermal performance. The findings contribute to a better understanding of how VTMS can be optimized for enhanced battery efficiency and life span.

2. METHODS

2.1 Experiment

This study investigates the thermal performance of a battery electric vehicle (BEV), focusing on the battery pack's cooling system, experimental setup, and driving conditions. Figure 1 shows an overview of the battery pack, including the coolant flow channels and sensor locations for temperature, pressure, and coolant flow rate.

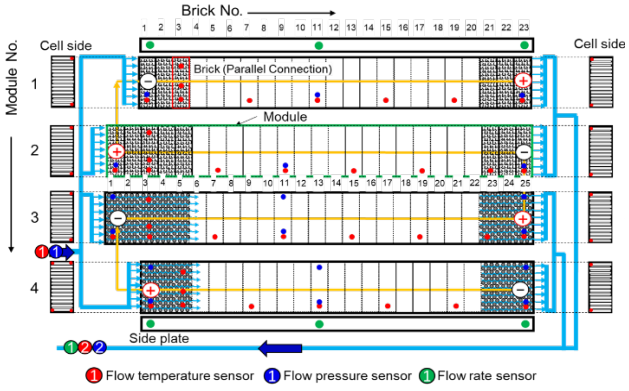

Fig. 1 High voltage battery pack architecture [4]

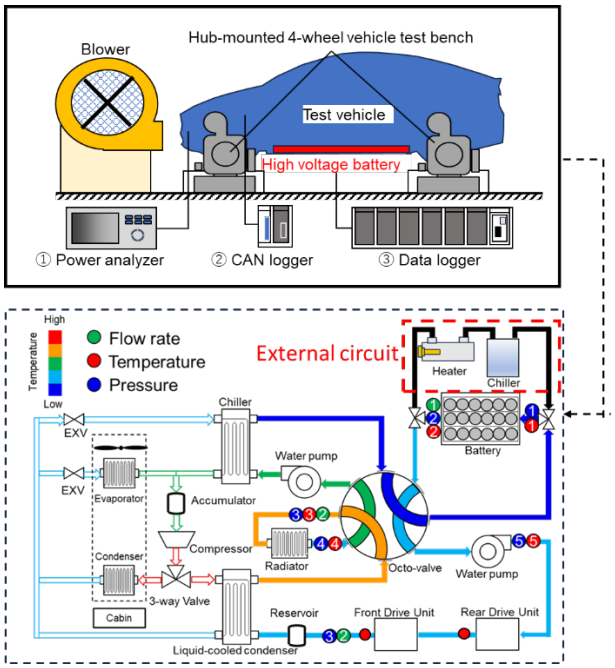

Fig. 2 Overview of experiment setup with thermal management System [4]

The thermal management system employs seven liquid cooling channels, alternated with insulating fiber spacers, to cool each module indirectly. Aluminum serpentine channels circulate ethylene-glycol coolant, promoting efficient thermal regulation across the modules. [5]

The experimental tests were conducted on a mid-size electric SUV using a chassis dynamometer, as shown in Figure 3. The test setup included a test room, a control room, and a blower to simulate airflow. Within the battery modules, eighty

Table 1. Experimental test conditions

Case No.	Condition	Ambient temperature $Tamb_i$ (°C)	Initial cell temperature Tc_i (°C)	Current (A)
1	Constant current discharge	25	25	150
2	Constant current discharge	25	25	50
3	Pressure drop	30	40	-
4	Pressure drop	18	-5	-

thermocouples were placed to monitor the temperature distribution. Electrical parameters were recorded with a power analyzer, while CAN data was captured via CAN logger. The control room enabled continuous monitoring and data collection throughout the driving cycles, with the driver following preset patterns assisted by driving aids [6][7] (refer to Figure 2).

Fig. 3 Test vehicle in chassis dynamometer setup

3. TEST CONDITIONS

The thermal performance was assessed under four test cases. Case 1 consisted of a constant discharge cycle, with ambient and initial cell temperatures of 25°C, an initial state of charge (SOC) of 80%, and a current of 150 A. Case 2 used the same conditions, except for a reduced current of 50 A. Cases 3 and 4 involved pressure drop tests, 30°C and 18°C ambient temperatures, respectively. In Case 3, the initial cell temperature was 25°C, the SOC was 0%, and the current was 0 A, while in Case 4, the initial cell temperature was also 25°C, with an ambient temperature of 18°C, and the SOC was 0%. All test conditions are summarized in Table 1.

4. EXPERIMENT RESULTS

The thermal performance of a high-voltage Battery Pack under Constant Discharge and Pressure Drop cycles is reported. The current and voltage are examined for Constant Discharge cycles. The average temperatures of the battery pack and module and temperature distributions on various bricks are explained. The pressure drop Inlet and outlet coolant temperature is discussed in the next section. This analysis offers insights into how these electrical parameters evolve under specific experimental conditions and drive cycles.

4.1 Electrical Parameters

This section reports the measured electrical parameters of the battery, such as voltage, current, and temporal variations across 2 different Constant Discharge cycles. The authors examine the impact of initial ambient and cell temperatures, as illustrated in Figure 4. In Cases 1 and 2, battery voltage, temperature, and SOC (State of Charge) demonstrate the effects of discharge current on performance. In Case 1, a high current of 150 A causes a rapid

voltage drop from 399 V to 319 V, a 10°C temperature rise, and fast SOC depletion from 81% to 19% over 3300 seconds. This indicates substantial thermal stress and faster energy consumption. Case 2, with a lower current of 50 A, shows a gradual voltage decline (396 V to 324 V), a smaller temperature increase (9°C), and slower SOC reduction over 10,000 seconds, highlighting better stability and energy conservation.

This comparison underscores the role of current regulation and thermal management for battery longevity. High currents accelerate heating and degradation, making effective cooling critical. Conversely, lower discharge rates extend runtime, improve temperature control, and support sustained power, emphasizing a need for adaptive battery management across applications.

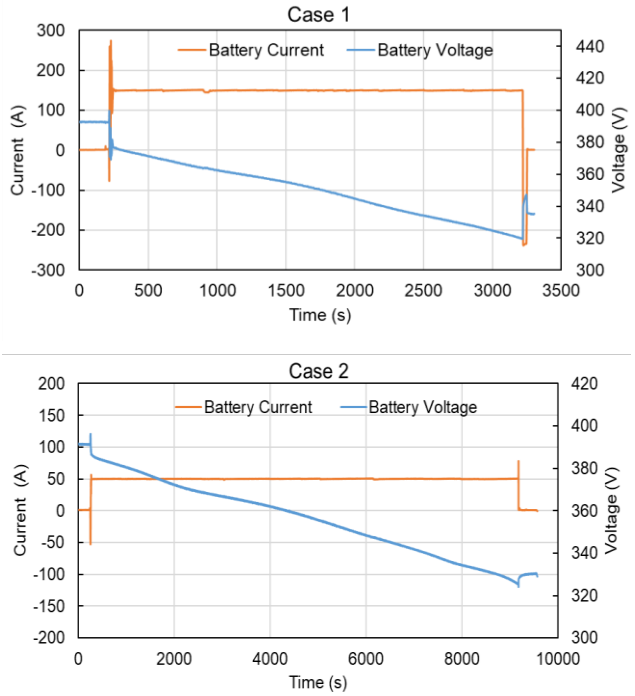

Fig. 4 Analysis of electrical parameters under constant current discharge experimental conditions

4.2 Thermal and Pressure Performance of Lithium Battery Packs Under Variable Initial Conditions

The first graph for Case 3 ($Tamb_i = 30$, $Tc_i = 40$) in Figure 5 shows the relationship between mass flow rate and battery cell temperature over time. Initially, the flow rate fluctuates between 19.95 and 0.04 L/min, stabilizing at approximately 15 L/min from 2625 to 5023 seconds. Meanwhile, the battery temperature gradually decreases from 40.7°C to 35.07°C, indicating effective heat dissipation during this steady-state period, which correlates with the stable coolant

flow rate. The second graph compares the battery's inlet and outlet pressures, with the inlet pressure rising sharply from -2.4 to 40.2 kPaG at 2556 seconds and remaining steady until 5000 seconds, then dropping to -2 kPaG. The stable inlet pressure and flow rate during these periods highlight the system's capacity to maintain cooling consistency under warmer conditions. Outlet pressure shows a similar trend.

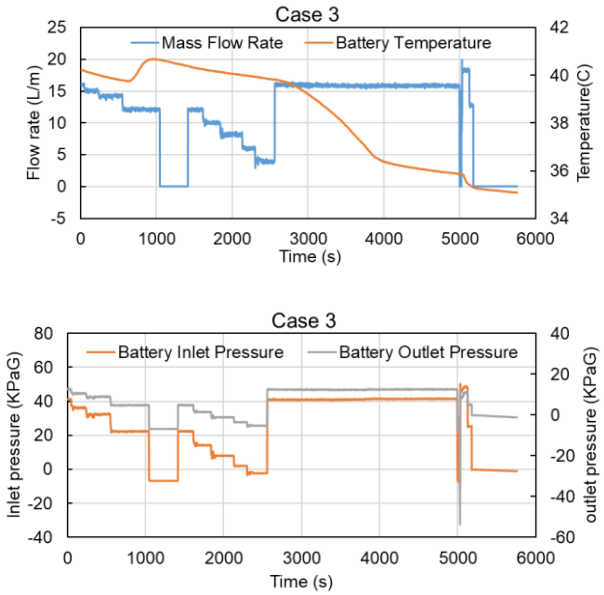

Fig. 5 Average battery temperature and coolant properties under Case 3 ($Tamb_i = 30$, $Tc_i = 40$)

In Case 4 ($Tamb_i = 18$, $Tc_i = -5$), illustrated in Figure 6 the initial cooling conditions are cooler, as shown in the first graph of the figure, we observe an intriguing pattern in battery temperature over time. Initially, the temperature rises gradually from -4.8°C to a peak of -4.1°C. This steady increase suggests a slow heat buildup within the battery. However, at 1418 seconds, a sudden, sharp drop back to -4.8°C indicates a rapid cooling effect. the initial cooling conditions are cooler, however, in the second graph, where both inlet and outlet pressures gradually decline. The outlet pressure experiences several steady phases (e.g., from 200 to 400 seconds at around 7.2 kPaG, followed by sharp drops until reaching -6.9 kPaG briefly. The second graph reveals a gradual temperature rise from -4.8°C to -4.1°C, alongside fluctuating flow rates from 13.13 to 0.65 L/min, showing a pattern like the inlet pressure. The prolonged steady states at lower temperatures indicate reduced cooling demand,

showing that stable cooling can be maintained with fewer fluctuations under lower ambient conditions.

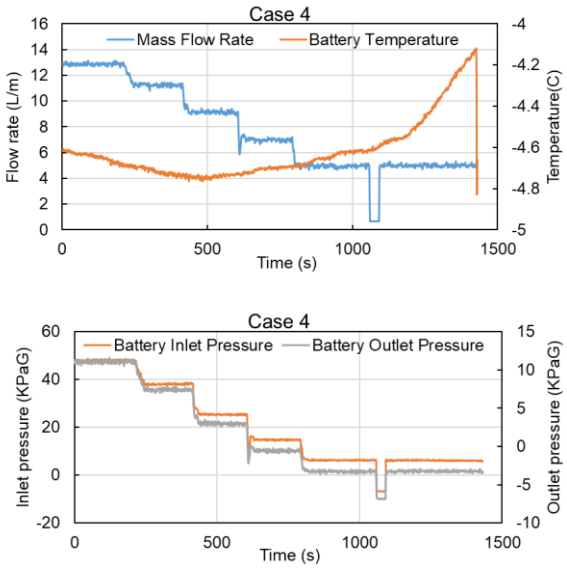

Fig. 6 Average battery temperature and coolant properties under Case 4 ($Tamb_i$ = 18, Tc_i = -5)

.

4.3 Coolant Circuit thermal Parameters under constant discharge conditions.

4.3.1 Case 1: $Tamb_i$ = 25, Current = 150A

Discharge current (150 A), the battery experienced a significant thermal load, causing the inlet temperature to rise from ~25°C to ~39°C as shown in Figure 7 and the outlet temperature to stabilize around 37°C. The cooling system dynamically adjusted the coolant mass flow rate, which peaked at ~9 L/min around 2000-2500 s, correlating with large temperature fluctuations. Despite these adjustments, the cooling system struggled to maintain stability, leading to sharp temperature rises beyond 3000 s as the flow rate declined. This suggests cooling limitations under high discharge conditions, requiring improvements in regulation strategies or additional cooling capacity. The strong correlation between temperature fluctuations and flow rate adjustments highlights the system's adaptive but insufficient response to high heat loads.

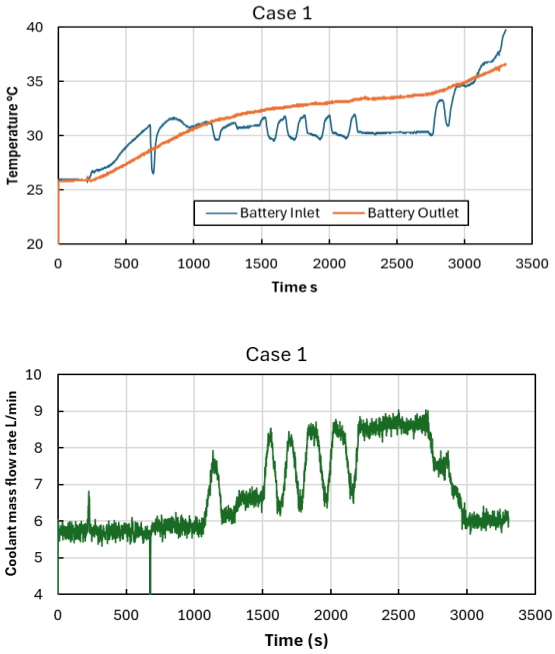

Fig. 7 Inlet and Outlet battery temperature and coolant Mass Flow Rate under Case 1 ($Tamb_i$ = 25, Current = 150A)

4.3.2 Case 2: $Tamb_i$ = 25, Current = 50A

The thermal load was reduced to a lower discharge current (50 A), leading to a gradual and stable temperature rise (inlet: ~25°C to ~32°C, outlet: ~30°C) as shown in Figure8. Unlike Case 1, the coolant mass flow rate adjustments were smoother and peaked at ~8 L/min, resulting in a more stable thermal response with fewer fluctuations. The cooling system effectively regulated battery temperatures without abrupt changes, ensuring better thermal stability. This indicates that lower discharge currents allow for more controlled cooling operations, optimizing energy efficiency. Comparing both cases, it is evident that higher discharge currents require aggressive and sometimes unstable cooling responses, whereas lower currents enable steady temperature management, improving system reliability.

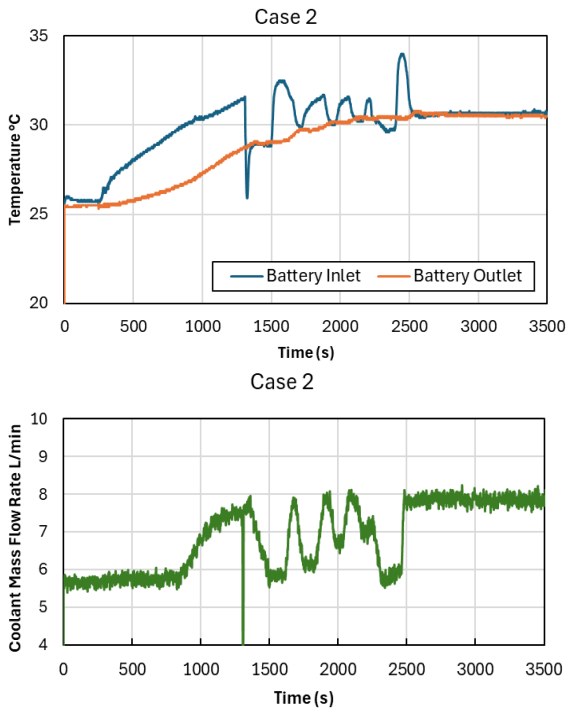

Fig. 8 Inlet and Outlet battery temperature and coolant Mass Flow Rate under Case 2 ($Tamb_i$ = 25, Current = 50A)

5. NUMERICAL METHOD

For Numerical Modeling, this study builds a previously developed and validated battery thermal management system model (coolant circuit) for SUVs, originally proposed by Ma et al. [8]. The original model was validated using data based on the worldwide Harmonized Light Vehicle Test cycle WLTC and Federal Test Procedure (FTP). In contrast, the present study focuses on constant discharge conditions to evaluate cabin temperature regulation under different operational conditions while maintaining consistency with the validated circuit data. To extend the previous model, a refrigerant and cabin circuit were incorporated into the previously validated battery temperature and experiment-based coolant circuit, aiming for further analysis.

5.1 Model

There is a need for full thermal system simulation due to the interconnectedness of the refrigerant and liquid coolant circuits used in advanced thermal management systems, especially in EVs. Therefore, the liquid coolant circuit was extended with a refrigerant circuit simulation capability.

In this work, the refrigerant circuit, in addition to the cabin circuit, is modeled in the GT-suite software package. the coolant circuit of the Octovalve thermal management system was used as a basis of the extension because of the validated battery modeling and temperature in addition, all model inputs and boundary conditions are taken from in-use vehicle chassis dynamometer tests.

Added refrigerant and cabin temperature both boundary conditions and data are from the GT-suite library. Since the added Refrigerant circuit is not based on an experiment like the coolant circuit the main objective of this model is to achieve a valid cabin temperature after adding the refrigerant circuit in addition to analyzing the interactions and thermal parameters between coolant and refrigerant circuits. Figure 9 represents an overview of the thermal management system.

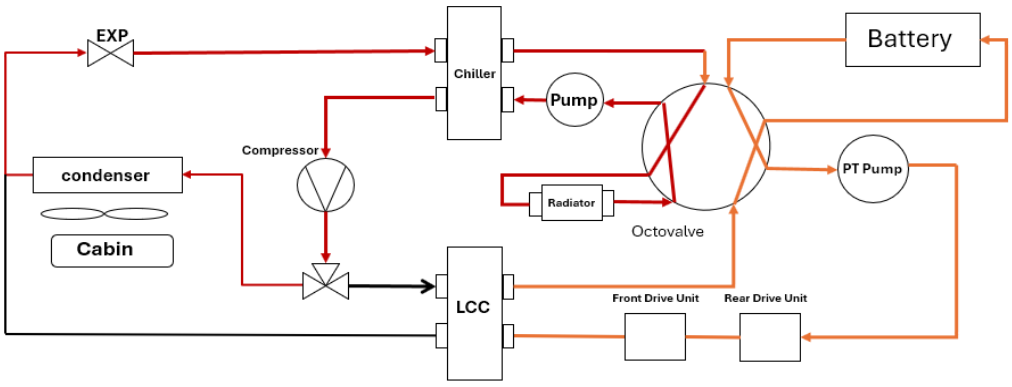

Fig. 9 overview of the thermal management system and the Octo valve position

5.2 Operating mode

The system under analysis has a total of 12 heating modes Wray et al [5], each with primary objectives, 4 of these modes (balancing) have been integrated into the model and Figure 9 shows the operating mode in this study. The radiator and chiller are in one circuit and the power and battery pack are connected in series to achieve the heat transfer between thermal reservoirs according to the operating condition. This mode was chosen to reduce heat exchange from the battery. In this mode evaporator and LLC are not active, this is why they are not integrated into the Figure 9.

6. SIMULATION RESULTS

6.1 Test Conditions

The simulation conditions were based on experimental data of coolant circuit, including battery output current, coolant inlet and outlet temperatures, volumetric flow rate, and outlet pressure, over a continuous period of 5800 seconds, as shown in Table 2. The primary objective of this simulation is to evaluate the refrigerant circuit's ability to maintain cabin comfort after integrating it with the already validated cooling circuit. To assess the system's heating capability, an ambient temperature of 12°C was selected under one constant discharge condition of 100A.

6.2 Coolant Circuit

As shown in Figure 10 the inlet temperature gradually increases and reaches a maximum of 25°C by the end of the simulation. The coolant outlet temperature follows a similar trend but remains consistently lower, stabilizing at 21°C, confirming continuous heat absorption from the battery. The coolant mass flow rate initially fluctuates before stabilizing at 0.053kg/s, indicating a controlled and regulated cooling operation. The initial transient behavior may be attributed to system stabilization, after which the mass flow rate remains nearly constant, ensuring a steady heat removal process.

Table 2 Simulation Conditions

Vehicle speed	Constant driving
Ambient condition	Winter
Ambient temperature	12 °C
Cabin condition	Heating
Target cabin temperature	25 °C
Refrigerant	R134a
Compressor	Scroll compressor

The temperature evolution of the four battery modules remains uniform, with minimal deviation between them. By the end of the simulation, the module temperatures reach approximately 23.5°C, demonstrating an even distribution of cooling across the system and preventing localized overheating.

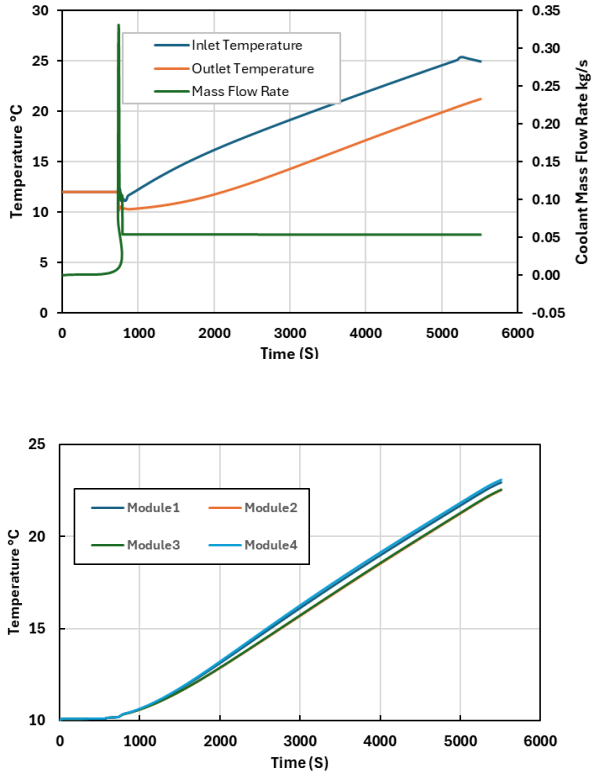

Fig. 10 Simulation results for coolant and battery temperature distributions across the four battery modules.

6.3 Refrigerant Circuit

6.3.1 Compressor

The compressor is responsible for the refrigerant flow rate in the HVAC circuit, on which the heat is exchanged, and the temperature variations. The compressor used for this study is a scroll compressor, specifications are listed in Table 3. For simulation results as Figure 11 shows, the pressure ratio of the compressor in refrigerant circuit experiences a sharp increase before stabilizing at 8.9 after approximately 800 seconds. This initial rise is due to transient conditions as the system adjusts to the thermal and flow dynamics of the refrigerant cycle. While the final stabilized pressure ratio is still relatively high, it remains within an expected range given the refrigerant cycle being numerically modeled rather than experimentally validated. While the coolant circuit components have experiment values, their interaction with a purely numerical refrigerant model led to deviations from expected pressure values.

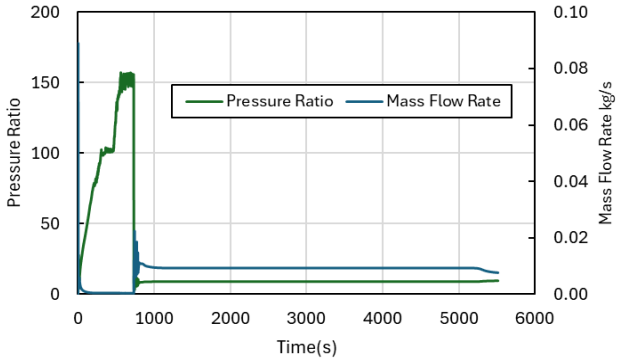

Fig. 11 Compressor Pressure Ratio and Mass Flow Rate VS Time

Table 3. Compressor Specifications

Type	Scroll compressor
Refrigerant	R134a
Displacement	41 cc
Inlet connection diameter	27 mm
Outlet connection diameter	23 mm

The refrigerant mass flow rate follows a similar trend,as seen in Figure 11 initially fluctuating before stabilizing at 0.1 kg/s. The early fluctuations correspond to the transient phase where the compressor adjusts to system conditions before reaching a steady-state operation. Stabilizing the mass flow rate indicates that the cooling system has reached a controlled operational state.

6.3.2 Compressor Controller

Before integrating a PID controller, the pressure ratio was significantly higher, reaching extreme values of 27. Such high fluctuations posed a risk to compressor stability and could lead to inefficiencies or system failures. To regulate the compressor operation and maintain cabin stability a PID controller was integrated into the system, as illustrated in Figure 12. The controller continuously adjusts compressor speed based on cabin air and Chiller outlet temperature feedback. The signal values (0 and 1) represent different control actions based on the detected cabin temperature and system conditions reached a controlled operational state.

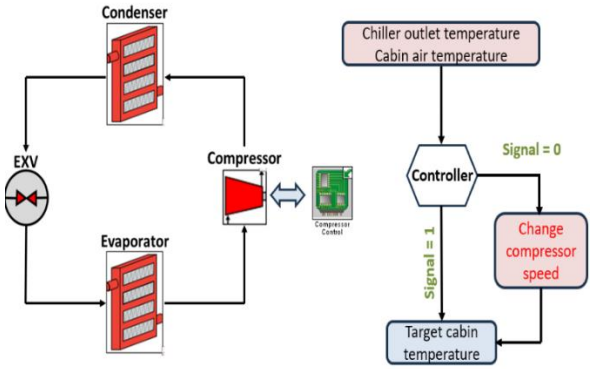

Fig. 12 Schematic representation of refrigerant circle integrating Compressor PID Controller.

6.3.3 Cabin Temperature

Figure 13 shows how the cabin temperature changes over time. After about 800 seconds, the temperature rises from 12°C to 25°C, reaching the desired comfort level. This confirms that the system effectively maintains cabin thermal comfort.

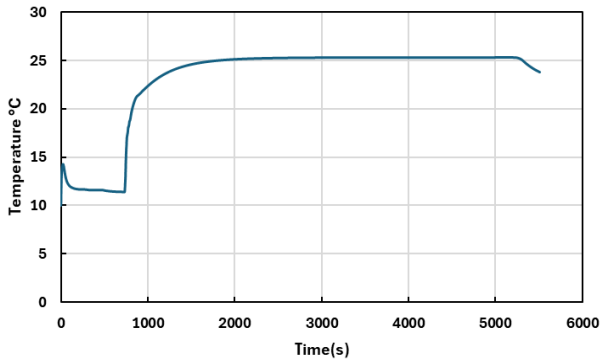

Fig.13 Cabin Temperature VS Time

7. CONCLUSION

In this study, thermal and pressure behavior in lithium-ion battery packs was analyzed under varying discharge currents and temperature conditions. The experimental results show that current and coolant mass flow rate significantly influence temperature and pressure stability, with higher currents demanding more active cooling and temperature management. Numerically this study builds upon the interactions and thermal parameters between coolant and refrigerant circuits to reach the objective of cabin temperature, however, other parameters objectives such as pressure ratio and refrigerant mass flow rate have not been achieved, in the future, experimental validation of the refrigerant circuit components is necessary to further enhance the accuracy and reliability of the model and further analysis for other refrigerant components such as the chiller and the condenser. A comprehensive validation approach, incorporating both numerical simulations and experimental data for the refrigerant cycle, would improve confidence in the full-system thermal management strategy for electric vehicles that includes coolant refrigerant and cabin circuits and allow for adjustments to improve the thermal management system of EVs after validation.

REFERENCES

(1) Chen, M., Ma, X., Chen, B., Arsenault, R. et al., “Recycling End Of-Life Electric Vehicle Lithium-Ion Batteries,” Joule 3, no. 11 (2019): 2622-2646.

(2) Tekin, S. and Türkakar, G., “Experimental Investigation of an Alternative Battery Pack Thermal Management System,” Journal of Energy Storage 59 (2023): 106485.

(3) Murali, G., Sravya, G.S.N., Jaya, J., and Vamsi, V.N., “A Review on Hybrid Thermal Management of Battery Packs and Its Cooling Performance by Enhanced PCM,” Renew. Sust. Energy. Rev. 150 (2021): 111513

(4) Sok, R., Kishida, K., Otake, T., Nandagopal, K. et al., "A Methodology to Develop and Validate a 75-kWh Battery Pack Model with Its Cooling System under a Real Driving Cycle," SAE Technical Paper 2024-37-0012, 2024

(5) Wray, A. and Ebrahimi, K., “Octo valve Thermal Management Control for Electric Vehicle,” Control for Electric Vehicle Energies 15 (2022): 6118.

(6)“Tesla Model Y Teardown: Electric Powertrain Technology,”https://www.marklines.com/en/report_all / Munro007_202105#report_area_3

(7)“TeslaPowershell,” https://en.wikipedia.org/wiki/Tesla_Powerwall.(accessed October 10, 2024)

(8) Ma, Y., Sok, R., Cui, E., Kishida, K. et al., "Development and Validation of a Battery Thermal Management Model for Electric Vehicles under Cold Driving," SAE Technical Paper 2023-01-1610, 2023

ACKNOWLEDGMENT

This work resulted from a joint project supported technically and financially by an undisclosed OEM partner. We thank our former graduate students – Kentaro Kishida (now in Toyota Motor Corp.), Yunkui Ma (now in Mercedez Benz Group, China), and Enbo Cui (now in AESC).